Customised design of antisense oligonucleotides targeting EGFR driver mutants for personalised treatment of non-small cell lung cancer

Trinh T. T. Tran,[a,l] Cao Dai Phung,[a,l] Brendon Z. J. Yeo,[a,l] Rebecca C. Prajogo,[a] Migara K. Jayasinghe,[a,b] Ju Yuan,[c] Daniel S. W. Tan,[c,d,e,f,g] Eric Y. M. Yeo,[a] Boon Cher Goh,[a,b] Wai Leong Tam,[b,c,h,i,**] and Minh T. N. Le[a,j,k,*]

[a]Department of Pharmacology and Institute for Digital Medicine, Yong Loo Lin School of Medicine, National University of Singapore, 16 Medical Drive, Singapore, 117600, Republic of Singapore
[b]Cancer Science Institute of Singapore, National University of Singapore, 14 Medical Drive, Singapore, 117599, Republic of Singapore
[c]Genome Institute of Singapore (GIS), Agency for Science, Technology and Research (A*STAR), 60 Biopolis Street, Genome, Singapore, 138672, Republic of Singapore
[d]Division of Medical Oncology, National Cancer Centre Singapore, 30 Hospital Blvd, Singapore, 168583, Republic of Singapore
[e]Duke-NUS Medical School, Republic of Singapore, 8 College Road, Singapore, 169857, Republic of Singapore
[f]Division of Clinical Trials and Epidemiological Sciences, National Cancer Centre Singapore, 30 Hospital Blvd, Singapore, 168583, Republic of Singapore
[g]Cancer and Therapeutics Research Laboratory, National Cancer Centre Singapore, 30 Hospital Blvd, Singapore, 168583, Republic of Singapore
[h]Department of Biochemistry, Yong Loo Lin School of Medicine, National University of Singapore, 16 Medical Drive, Singapore, 117600, Republic of Singapore
[i]NUS Centre for Cancer Research, Yong Loo Lin School of Medicine, National University of Singapore, 14 Medical Drive, Singapore, 117599, Republic of Singapore
[j]Department of Surgery, Yong Loo Lin School of Medicine, National University of Singapore, 1E Kent Ridge Road, Singapore, 119228, Republic of Singapore
[k]Institute of Molecular and Cell Biology (IMCB), Agency for Science, Technology and Research, (A*STAR), 61 Biopolis Street, Proteos, Singapore, 138673, Republic of Singapore

eBioMedicine
2024;108: 105356
Published Online xxx
https://doi.org/10.1016/j.ebiom.2024.105356

Summary

Background Tyrosine kinase inhibitors (TKIs) are currently the standard therapy for patients with non-small cell lung cancer (NSCLC) bearing mutations in epidermal growth factor receptor (*EGFR*). Unfortunately, drug-acquired resistance is inevitable due to the emergence of new mutations in *EGFR*. Moreover, the TKI treatment is associated with severe toxicities due to the unspecific inhibition of wild-type (WT) EGFR. Thus, treatment that is customised to an individual's genetic alterations in *EGFR* may offer greater therapeutic benefits for patients with NSCLC.

Methods In this study, we demonstrate a new therapeutic strategy utilising customised antisense oligonucleotides (ASOs) to selectively target activating mutations in the *EGFR* gene in an individualised manner that can overcome drug-resistant mutations. We use extracellular vesicles (EVs) as a vehicle to deliver ASOs to NSCLC cells.

Findings Specifically guided by the mutational profile identified in NSCLC patients, we have successfully developed ASOs that selectively inhibit point mutations in the *EGFR* gene, including L858R and T790M, while sparing the WT *EGFR*. Delivery of the *EGFR*-targeting ASOs by EVs significantly reduced tumour growth in xenograft models of EGFR-L858R/T790M-driven NSCLC. Importantly, we have also shown that *EGFR*-targeting ASOs exhibit more potent anti-cancer effect than TKIs in NSCLC with *EGFR* mutations, effectively suppressing a patient-derived TKI-resistant NSCLC tumour.

Interpretation Overall, by harnessing the specificity and efficacy of ASOs, we present an effective and adaptable therapeutic platform for NSCLC treatment.

*Corresponding author. Department of Pharmacology and Institute for Digital Medicine, Yong Loo Lin School of Medicine, National University of Singapore, 16 Medical Drive, Singapore, 117600, Republic of Singapore.
**Corresponding author. Cancer Science Institute of Singapore, National University of Singapore, 14 Medical Drive, Singapore, 117599, Republic of Singapore.
E-mail addresses: phcltnm@nus.edu.sg (M.T.N. Le), tamwl@gis.a-star.edu.sg (W.L. Tam).
[l]Trinh T.T. Tran, Cao Dai Phung, and Brendon Z.J. Yeo contributed equally to this work.

Funding This study was funded by Singapore's Ministry of Health (NMRC/OFIRG/MOH-000643-00, OFIRG21nov-0068, NMRC/OFLCG/002-2018, OFYIRG22jul-0034), National Research Foundation (NRF-NRFI08-2022, NRF-CRP22-2019-0003, NRF-CRP23-2019-0004), A*STAR, and Ministry of Education.

Keywords: Non-small cell lung cancer; EGFR; Extracellular vesicles; Antisense oligonucleotides; Cancer therapy

Research in context

Evidence before this study

Non-small cell lung cancer (NSCLC) is usually diagnosed at a late stage and has a poor prognosis. NSCLC tumours are genetically heterogenous but rely on certain oncogenes to proliferate and spread. In the Asian population, *EGFR* is the most common hotspot of mutations, accounting for almost 50% of patients with NSCLC. Patients who are EGFR-positive respond well to TKIs, but resistance and relapse are inevitable due to the rapid evolution of mutations at the drug-binding site. Antibodies targeting EGFR show only a modest effect and benefit only a small cohort of patients. An alternative approach to target EGFR is to suppress its gene expression using antisense oligonucleotides (ASOs). However, the highly anionic charge makes it difficult for naked ASOs to efficiently enter cells. Our group has recently developed a new platform for efficient delivery of nucleic acid drugs using red blood cell-derived extracellular vesicles (RBCEVs). We have successfully utilized RBCEVs for ASO delivery to tumor cells in various models of leukemia and solid cancers.

Added value of this study

Here, we present a novel therapeutic strategy that employs customized ASOs to selectively target activating mutations in the EGFR gene and deliver these ASOs to NSCLC cells using RBCEVs. Based on the mutational profile of NSCLC patients, the ASOs were designed to selectively target and inhibit the *EGFR* L858R and T790M mutations, while leaving the wild-type *EGFR* unaffected. Surface functionalization of RBCEVs with a tumour-targeting nanobody further enhances their specificity, leading to reduced tumour growth in xenograft mouse models. Importantly, ASO-loaded RBCEVs exhibit potent anti-cancer effects, compared to TKIs, and effectively suppress the growth of a patient-derived TKI-resistant NSCLC tumour.

Implications of all the available evidence

We have successfully developed an EV-delivered ASO therapeutic platform that is both effective and versatile, with the potential to advance personalised and precision medicine for the treatment of NSCLC.

Introduction

Non-small cell lung cancer (NSCLC) is the predominant subtype, accounting for approximately 80% of all lung cancer cases, and is associated with a poor 5-year survival rate.[1] While NSCLC cells exhibit genetic heterogeneity, they are addicted to certain driver oncogenes for survival and progression, such as mutant epidermal growth factor receptor (*EGFR*), Kirsten rat sarcoma virus (*KRAS*) and anaplastic lymphoma kinase (*ALK*).[2] These genetic alterations offer specific molecular targets for therapeutic intervention in NSCLC treatment. For instance, EGFR tyrosine kinase inhibitors (TKIs), such as erlotinib and gefitinib, have shown impressive responses in patients of NSCLC with activating *EGFR* mutations. However, cancer relapse eventually happens within 10–14 months of the TKI treatment due to the inevitable development of resistance.[3] The cause of TKI-acquired resistance is the emergence of the T790M gatekeeper mutation in the catalytic domain of the EGFR kinase. More than half of patients experiencing a relapse in cancer development who initially received first or second-generation TKIs develop this mutation, which enhances their affinity to adenosine triphosphates (ATPs) and reduces their binding to TKIs.[4,5] The third-generation TKI, Osimertinib, which irreversibly binds to EGFR with T790M at 200 times stronger than to the wild-type EGFR,[3] is superior to earlier generations of TKIs in prolonging survival and has become the current standard of care for EGFR-addicted tumours.[6] Unfortunately, resistance to Osimertinib has emerged due to the quick development of a mutation in the EGFR residue C797 within the ATP-binding site.[7] In addition to TKIs, anti-EGFR antibodies, such as Cetuximab, block epidermal growth factor (EGF) binding, leading to the nonspecific internalization and degradation of EGFR. However, they only elicit a modest impact on a specific sub-population of patients.[8]

In addition to small molecules or protein drugs, antisense oligonucleotides (ASOs) have attracted significant attention due to their simplicity and versatility in designing, screening, and testing. By regulating gene expression at mRNA levels, ASOs can overcome limitations associated with small molecules in targeting undruggable molecules that lack active binding pockets; and outcompete monoclonal antibodies in targeting intracellular proteins. Moreover, ASO sequences are easily customised to target any mutated gene, contributing to a significant progress in precision and

personalised medicine. ASO drugs have demonstrated safety and therapeutic efficacy and have received approval for treatments against several rare diseases.[9,10] However, the delivery of ASOs to target sites and their cellular uptake face significant challenges due to their undesirable *in vivo* biodistribution, susceptibility to degradation, and low cell permeability owing to their negative charges. Therefore, efficient carriers for ASO therapeutics are highly desirable to advance their potential.

Recently, natural nanocarriers have been increasingly used for nucleic acid delivery, with extracellular vesicles (EVs) being the most prominent example. Secreted by cells, facilitating cell-to-cell communication, and possessing the ability of tissue-homing, EVs are actively investigated in various clinical trials for the treatment of infectious diseases and degenerative diseases, or as anti-cancer drug carriers.[11] In our previous studies, we have demonstrated that red blood cell-derived EVs (RBCEVs) can be produced at a large quantity and effectively loaded with various types of nucleic acid therapeutics.[12] Furthermore, RBCEVs can be conjugated with targeting moieties, which substantially enhance their biodistribution to target tissues and their uptake by target cells.[13,14] In this study, we employed RBCEVs to transport therapeutic ASOs to NSCLC cells. Guided by the mutational profile identified in tumour cells from patients with NSCLC, we have successfully developed ASOs targeting specific *EGFR*'s point mutations, L858R and T790M, with minimal effect on the WT *EGFR*. ASO-loaded RBCEVs were taken up by NSCLC cells, suppressing EGFR protein expression in NSCLC cells harbouring L858R/T790M co-mutation, leading to a potent anti-cancer effect compared to TKI treatments. We further showed that surface functionalization of RBCEVs with a cancer-targeting nanobody resulted in enhanced delivery of the ASO to cancer cells *in vivo*, leading to improved anti-cancer efficacy.

Methods

Purification of human RBCEVs

Blood samples were obtained from healthy donors via Innovative Research Inc. (USA) with informed consent. RBCEVs were then purified from human red blood cells (RBCs) in collaboration with ESCO Aster (Singapore), following our established protocol[12] according to the approval by our University Institutional Review Board (IRB) (NUS-IRB Reference Code: LH-19-058E). Briefly, RBCs were separated from the plasma by centrifugation at 1000×g for 8 min at 4 °C, followed by washing with PBS thrice at the same speed. White blood cells were removed using leukodepletion filters (Nigale, China). The resulting RBC suspension was collected in Nigale buffer (0.2 g/L citric acid, 1.5 g/L sodium citrate, 7.93 g/L glucose, 0.94 g/L sodium dihydrogen phosphate, 0.14 g/L adenine, 4.97 g/L sodium chloride, 14.57 g/L mannitol), diluted in CPBS (PBS containing 0.1 mg/mL calcium chloride), and incubated overnight with 10 μM calcium ionophore (Sigma–Aldrich, USA) at 37 °C with 5% CO_2 to induce vesiculation. RBCs and cell debris were subsequently removed through sequential centrifugation. The supernatant, containing RBCEVs, was filtered through a 0.45 μm filter membrane, followed by ultracentrifugation at 50,000×g for 1 h. The pelleted RBCEVs were further purified by ultracentrifugation at 50,000×g overnight with a 60% sucrose cushion to completely remove protein contaminant. Finally, the purified RBCEVs were resuspended in PBS containing 4% trehalose (Sigma–Aldrich) and stored at –80 °C.

RBCEV characterization

Since haemoglobin (Hb) is the major component of RBCEVs, Hb content was used to indicate the quantity of RBCEVs in this study. Hb content was determined using a NanoDrop 2000 spectrophotometer (Thermo-Fisher Scientific, USA) by measuring absorbance at isosbestic wavelengths for Hb and Oxy-Hb (420 and 586 nm, respectively).

The morphology of RBCEVs was characterised using TEM. Briefly, RBCEVs were fixed with 2% paraformaldehyde, mounted on glow-discharged copper grids, and washed. Subsequently, they were incubated with 3% uranyl acetate for negative staining, followed by washing with water, and air-drying. Images of RBCEVs were captured using a TEM instrument at 100 kV (Tecnai G2, FEI/Philips, USA).

Surface charge, polydispersity index (PDI), and particle size distribution of RBCEVs were characterised by dynamic light scattering (DLS) using Zetasizer Ultra instrument (Malvern Panalytical, UK). For surface charge measurement, RBCEVs were diluted in 10 mM HEPES buffer pH 7.4 and loaded into a capillary zeta cell (DTS1070, Malvern Panalytical, UK). For PDI and size distribution, RBCEVs were diluted in PBS and loaded into a particle size analytical cuvette (DTS0012, Malvern Panalytical, UK).

For nano-flow cytometric analysis, RBCEVs were stained with biotinylated anti-human GPA primary antibody (Biolegend, USA) and then stained with streptavidin-Alexa Fluor 488-conjugated secondary antibody (Abcam, USA). The stained RBCEVs were washed with PBS twice by centrifuging at 21,000×g, diluted with PBS, and analysed using a Flow Nanoanalyzer system (NanoFCM, UK). Plots were generated using FlowJo V10 software (BD Biosciences, USA).

ASOs, primers, and nanobody synthesis

ASOs against *EGFR* L858R or T790M mutations, negative control ASO (NC ASO, 5′-CGACTATACGCGCAATATGG-3′), fluorescein amidites-labelled NC ASO (FAM-ASO), and Alexa Fluor 488-labelled NC

ASO (AF488-ASO) with 2′-O-methoxyethyl (MOE), Phosphorothioate (PS), and Locked Nucleic Acid (LNA) modifications, and qPCR primers (Table S2) were synthesised by Integrated DNA Technologies (USA).

The anti-EGFR nanobody (α-EGFR-VHH) and anti-mCherry nanobody (α-mCherry-VHH) were cloned with a 6xHis tag and a FLAG tag and purified according to our previously published method.[13]

ASO loading into RBCEVs

1 μg of ASO was loaded into 50 μg RBCEVs using REG-1 transfection reagent (Carmine Therapeutics, Singapore) according to the manufacturer's instructions. Briefly, REG-1 and ASOs diluted in Opti-MEM medium (ThermoFisher Scientific, USA) were mixed at a final concentration of 70 μg/mL for REG-1 and 10 μg/mL for ASO, respectively. The mixture was incubated at room temperature for 10 min to facilitate complex formation between ASOs and REG-1. Thereafter, 50 μg of RBCEVs, diluted in Opti-MEM medium to a concentration of 1 mg/mL, were mixed with the REG-1/ASO complex and incubated at 37 °C in a HulaMixer (ThermoFisher Scientific, USA) for 30 min and on ice for 10 min to facilitate the loading of ASO into the RBCEVs. Afterwards, free ASOs and transfection reagents were washed away by centrifuging at 21,000×*g* for 30 min.

To quantify the ASO loading efficiency into RBCEVs, 20 μg of RBCEVs loaded with ASOs were resuspended in 0.1% Triton-X (Sigma–Aldrich, USA) for 5 min at room temperature, and subsequently with heparin sulfate at a final concentration of 20 mg/mL for 1 h at 37 °C with shaking at 100 rpm. After incubation, a 6X gel loading dye (New England Biolabs, USA) was added and the resulting mixture was loaded onto a 2% Tris-acetate-EDTA agarose gel with GelRed® nucleic acid gel stain (Sigma–Aldrich, USA), separated at 100 V for 15 min and visualised with a ChemiDoc™ XRS + imaging system (Bio-Rad Laboratories, USA). The band fluorescence intensity was quantified using ImageJ v1.8.0.

RBCEV surface modification

Strain promoted alkyne–azide cycloaddition (SPAAC) click chemistry was employed to conjugate α-EGFR-VHHs onto RBCEVs. Briefly, RBCEVs were incubated with Dibenzocyclooctyne sulfotetrafluorophenyl (DBCO-STP) ester (Click Chemistry Tools, China) at a final concentration of 20 mg/mL for RBCEVs and 2 mM for DBCO-STP, respectively, for 2 h at room temperature in PBS pH 8.0. Subsequently, 1M Tris pH 8.0 (Sigma Aldrich, USA) was added to the reaction at 10% (v/v) for 5 min at room temperature to quench remaining free unreacted STP-ester groups. The DBCO-tagged RBCEVs (DBCO-EVs) were subsequently washed four times in PBS pH 8.0 by centrifuging at 21,000×*g* for 20 min at 4 °C to remove the quenched free ester. Concurrently, α-EGFR-VHHs was incubated with 6-Azidohexanoic Acid STP (Azide-STP) ester (Click Chemistry Tools, China), at a final concentration of 5.5 mg/mL for α-EGFR-VHHs and 2 mM for Azide-STP, for 2 h at room temperature. Excess non-reacted Azide-STP ester was removed using a Zeba Spin Desalting Column (7K MWCO, ThermoFisher Scientific, USA). Subsequently, DBCO-EVs were incubated with the Azido-VHHs at a final concentration of 10 mg/mL for DBCO-EVs and 150 μM for Azido-VHH, respectively, overnight at 4 °C. The α-EGFR VHH-conjugated EVs (EGFR-VHH-EVs) were washed four times with PBS pH 8.0 by centrifuging at 21,000×*g* for 20 min at 4 °C. The successful conjugation was confirmed by Western blotting.

Western blot

RBCEVs, RBCs and other cancer cell samples were lysed in Pierce radio-immunoprecipitation assay (RIPA) lysis and extraction buffer (ThermoFisher Scientific, USA) supplemented with 1 mM phenylmethylsulfonyl fluoride (PMSF) protease inhibitor (ThermoFisher Scientific, USA) on ice for 5 and 20 min, respectively. Following lysis, the cell lysate was centrifuged at 12,000×*g* for 5 min, and the protein-containing supernatant was collected. Protein concentrations were quantified using a Pierce BCA protein assay kit (New England Biolabs, UK) following the manufacturer's instruction. Subsequently, 4x Laemmli buffer (Bio-Rad Laboratories, USA) was added to 30 μg of protein lysate from cells or RBCEVs and heated at 95 °C for 7 min. The protein lysates were loaded into 10% polyacrylamide gels and separated along with a protein standard (Precision Plus Protein Kaleidoscope-prestained protein ladder, Bio-Rad Laboratories, USA). The separated proteins were then transferred to a polyvinylidene fluoride (PVDF) membrane (Merck Millipore, USA), followed by blocking with Tris-buffered saline containing 0.1% Tween-20 (TBST) and 5% BSA for 1 h at room temperature (RT). The membranes were incubated overnight at 4 °C with primary antibodies (Table S3), including anti-human BAND 3 antibody (Santa Cruz, Cat #: sc-133190, RRID #AB_2123479, dilution 1:1000), anti-human STOMATIN antibody (Santa Cruz, Cat #: sc-376869, 1:1000), anti-ALIX antibody (Santa Cruz, Cat #: sc-53538, RRID AB_673821, dilution 1:500), anti-TSG101 antibody (Santa Cruz, Cat #: sc-7964, RRID AB_671392, dilution 1:500), anti-human HBA antibody (Santa Cruz, Cat #: sc-21005, RRID AB_647937, dilution 1:1000), anti-human GPA antibody (Biolegend, Cat #: 306602, RRID AB_314620, dilution 1:500), anti-human β-actin antibody (Proteintech, Cat #: HRP-60008, RRID AB_2819183, dilution 1:5000), anti-calnexin antibody (Santa Cruz, Cat #: sc-23954, RRID AB_626783, dilution 1:500), and anti-human GAPDH antibody (Proteintech, Cat #: HRP-60004, RRID AB_2737588, dilution 1:5000), anti-human EGFR antibody (Cell Signaling, Cat #: 4267, RRID

AB_2895042), anti-human phospho-EGFR antibody (Cell Signaling, Cat #: 3777, RRID AB_2096270), anti-human ERK1/2 antibody (Cell Signaling, Cat #: 4695, RRID AB_390779), anti-human AKT antibody (Cell Signaling, Cat #: 9272, RRID AB_329827). To determine efficacy of nanobody conjugation onto RBCEVs, 100 µg of conjugated RBCEV lysate and various EGFR-VHH standards were separated in 10% polyacrylamide gels, transferred to a PVDF membrane, and blocked with 5% BSA in TBST as described above. The membrane was then incubated overnight at 4 °C with anti-FLAG antibody (Abkkine, Cat#: A02010, dilution 1:5000). After washing with TBST, the membranes were incubated with appropriate horseradish peroxidase (HRP)-conjugated anti-rabbit or anti-mouse secondary antibodies (Abcam, USA, dilution 1:10,000), followed by incubation with a HRP substrate (WesternBright Sirius Chemiluminescent Detection Kit, Advansta, USA). The blots were imaged using a ChemiDoc™ XRS + imaging system (Bio-Rad Laboratories, USA).

Cell culture

4T1 (RRID: CVCL_0125), A549 (RRID: CVCL_0023), and H1975 (RRID: CVCL 1511) cells were obtained from the American Tissue and Cell Collection (ATCC, USA) and cultured in Roswell Park Memorial Institute (RPMI) 1640 with L-Glutamine (Biowest, France) supplemented with 10% (v/v) heat-inactivated fetal bovine serum (Biowest, France), 1% penicillin-streptomycin (Gibco, USA) in a humidified incubator at 37 °C with 5% CO_2. Mycoplasma testing of these cell lines is conducted regularly with a commercial obtained mycoplasma detection kit (Applied Biological Materials Inc., Canada).

Patient sample processing

Among the patients diagnosed with EGFR mutant LUAD at the National Cancer Centre Singapore, which underwent surgical resection of their tumours, three patients, in which two developed *EGFR* L858R mutation (A014, A428) and one developed *EGFR* T790M mutation (A003), were selected for this study under consent (relevant clinical information of each patient is provided in Fig. S1). The protocol for using human samples in this study was approved by A*STAR Institutional Review Board (IRB, Singapore, IRB reference code: 2024-015). Tumour biopsies or sectors were freshly processed for cell culture.

The fresh tumour biopsy or sector was digested with 1 mg/mL collagenase IV (Gibco) and 1 mg/mL dispase II (Thermo Fisher Scientific, USA) in F12 media (Thermo Fisher Scientific, USA) for 2 h with shaking in a 37 °C incubator. Cell suspension was then passed through a 70 µm cell strainer and centrifuged for 3 min at 1500 rpm. Cells were then washed twice and resuspended in media before seeding on irradiated 3T3 feeders as previously described.[15] When the cells reached confluence, sub-culturing was carried out by first lifting the feeders using 0.05% trypsin for 2 min. After removing feeder cells, 0.05% trypsin was added to detach tumour progenitor cells. All cells were routinely tested and verified to be free of mycoplasma contamination.

RNA extraction and real-time quantitative PCR (qPCR)

TRIzol reagent (ThermoFisher Scientific, USA) was used to isolate total RNA from treated cells following the manufacturer's protocol. The extracted RNA was converted into cDNA using a high-capacity cDNA reverse transcription kit (ThermoFisher Scientific, USA) according to the manufacturer's instructions. qPCR reactions to quantify the expression level of target mRNA were performed on a QuantStudio 6 Flex Real-Time PCR system (Life Technologies, USA) using Ssofast® Green qPCR kit (Bio-Rad Laboratories, USA), normalised to the expression of GAPDH.

Sanger sequencing

Sanger sequencing was carried out to validate EGFR mutations in patient-derived tumour cells and H1975 cells. RNA was extracted from these cells, followed by the cDNA synthesis as described previously. PCR amplification of the region covering from exon 18 to exon 21 was performed using the following primer pair: Exon 18–22 forward 3′-CTTACACCCAGTGGAGAAGC-5′, and Exon 18–22 reverse 3′-CAATGCCATCCACTTGATAGG-5' (Table S1). The amplicons were purified using the GeneJet PCR purification kit (Thermo Fisher Scientific, USA), run on 2% agarose gel for the product size confirmation, and then sent to Macrogen (Singapore) for Sanger sequencing.

Cell proliferation assay

To assess the anti-tumour effect of ASOs delivered by RBCEVs, H1975 cells were seeded in a 96-well plate at a density of 1.0 x 10^4 cells per well, prior to incubation with TKIs (HaoYuan ChemExpress, China), or RBCEVs loaded with either *EGFR* L858R ASO or *EGFR* T790M ASO at equivalent molar doses of ASO and TKIs. 48 h post-treatment, treated cells were incubated with 10% (v/v) of CCK-8 reagent (MedChemExpress, USA) and absorbance at 450 nm was measured using a microplate reader (Tecan, Switzerland). Relative cell count was determined according to the following equation:

$$\text{Relative cell count (\%)} = [(OD450_{(\text{Treated sample})} - OD450_{(\text{blank})}) / (OD450_{(\text{Untreated sample})} - OD450_{(\text{blank})})] \times 100\%$$

Apoptosis assay

Apoptosis of H1975 cells following treatment with TKIs and ASO-loaded RBCEVs were detected by Annexin V (Biolegend, USA) and SYTOX Blue (ThermoFisher Scientific, USA) staining. Briefly, H1975 cells were seeded at a density of 1.0 x 10^5 cells per well in a 24-well

plate overnight. Then, the cells were treated with 200 nM of Icotinib, Afatinib, Osimertinib, or ASO loaded in RBCEVs. After 24 h, treated cells were harvested and stained with Annexin V and SYTOX Blue following the manufacturer's instructions. The stained cells were finally analysed using a Flow Cytometer (CytoFlex, Beckman Coulter, USA).

Cellular uptake studies

The uptake of ASO-loaded RBCEVs was investigated by flow cytometry and confocal laser scanning microscopy (CLSM). For flow cytometric analysis, the H1975 cells were seeded into 12-well plates at a density of 1.0 x 10^5 cells/well overnight. Thereafter, the cells were treated with RBCEVs loaded with AF488-ASO at different RBCEV concentrations and incubation times. After washing thrice with PBS, the cells were harvested and analysed for their fluorescence intensity using a Flow Cytometer (CytoFlex, Beckman Coulter, USA).

To visualise the cellular uptake of ASO-loaded EVs, H1975 cells were cultured in 6-well plates covered by microscope coverslips at a density of 2.0 x 10^5 cells/well. The next day, RBCEVs loaded with AF488-ASO were added to the cells at an RBCEV concentration of 30 μg/mL and incubated at 37 °C for 1 h, followed by the addition of 2 nM Lysotracker Red (ThermoFisher Scientific, USA) for an additional 10 min. Cells were gently washed twice with PBS and fixed with 4% paraformaldehyde, prior to incubation with 10 μg/mL Hoechst 33342 (ThermoFisher Scientific, USA). Finally, the stained cells were mounted on a glass slide and observed under a CLSM (Zeiss LSM710, Germany).

Animal studies

All mouse experiments were performed in accordance with experimental protocols approved by the Institutional Animal Care and Use Committee (IACUC) of the National University of Singapore (iORC Reference No.: R19-1195). NSG-SGM3 (NSGS) mice (RRID: IMSR_JAX: 013062) and BALB/c nude mice (RRID: IMSR_JAX: 000651) were purchased from the Jackson Laboratory (USA). The mice were housed in pathogen-free animal facilities and fed a standard diet. Experiments were conducted in a blind manner. Mice of similar ages were tagged and grouped randomly into control or test treatments.

Biodistribution studies

To investigate the delivery of ASOs to tumour cells by RBCEVs and EGFR-VHH-conjugated RBCEVs *in vivo*, H1975 cells were transduced with a lentiviral vector (pLenti-mCherry-luc, Addgene, USA), selected with puromycin (Santa Cruz, USA) and sorted using Aria II sorter (BD Biosciences, USA) to generate a stable luciferase and mCherry-expressing H1975 cell line (H1975-Luc-mCherry) (Fig. S6). A total of 1.0 x 10^6 $H^{19}75$-Luc-mCherry cells were injected intravenously in 8-week-old NSGS mice. After 6 weeks, the mice were intra-peritoneally injected with D-luciferin (PerkinElmer, USA) and subjected to IVIS imaging to monitor tumour growth in the lung. Tumour-bearing mice were then intratracheally treated with RBCEVs or EGFR-VHH-EVs loaded with FAM-ASO at a dose of 100 μg/kg of ASO. Following 3 h post-administration, mice were sacrificed, and lungs were harvested. Single lung cells were dissociated using a gentleMACS dissociator (Miltenyi, Germany) and incubated with collagenase IV (Life Technologies, USA) for 40 min at 37 °C with shaking. The cells were passed through a 70 μm cell strainer and centrifuged at 500×*g* for 5 min. RBCs were lysed using ACK lysis buffer (ThermoFisher Scientific, USA). The resultant single cells were washed with PBS and subjected to flow cytometric analysis using a Flow Cytometer (CytoFlex, Beckman Coulter, USA).

Intrapulmonary targeted delivery of ASO-loaded RBCEVs to orthotopic cell line xenograft model

NSGS mice bearing H1975-Luc-mCherry tumour at the lung were generated as described above. Mice with similar bioluminescence intensity were divided into three groups (n = 4, denoted as day 1), including RBCEVs loaded with NC ASO (NC ASO-EVs), RBCEVs loaded with L858R ASO (L858R ASO-EVs), and EGFR-VHH-conjugated RBCEVs loaded with L858R ASO (L858R ASO-VHH-EVs), and intratracheally administrated at a dose of 200 μg/kg of ASO, repeated at 3-days intervals. On day 15, mice were sacrificed, and lung tissues were collected for subsequent experiments.

Intra-tumoural administration of ASO-loaded RBCEVs to patient-derived xenograft model

Female 7-week-old BALB/c nude mice were subcutaneously injected with 1.0 x 10^6 A014 patient-derived cancer cells at the right flank. When tumour volume reached approximately ~50 mm^3, the mice were randomly divided into two groups (n = 4, denoted as day 1) and intratumourally injected with NC ASO-EVs (control) or L858R ASO-EVs at a dose of 50 μg/kg ASO, repeated at 2-days intervals for three weeks. During the study period, the length and width of tumours were measured using a digital calliper. The tumour volume (mm^3) was calculated using the formula: $V = 1/2 \times \text{length} \times \text{width}^2$. On day 22, the mice were sacrificed, and tumours were harvested for subsequent analysis.

Immunofluorescence, immunohistochemistry, and TUNEL assay

The isolated tissues were fixed with 10% neutral buffered formalin solution (Sigma Aldrich, USA) and subjected to a serial dehydration with ethanol (70%, 80%, 90%, and 100%) using a TP1020 tissue processor (Leica, C). The samples were then subjected to three baths in Histo-Clear (National Diagnostics, USA) for 1.5 h at 37 °C each, before incubation in three baths of paraffin wax (Thermo Fisher Scientific) for 1 h at 62 °C each.

Paraffin blocks were sectioned at 4 μm using a RM2255 rotary microtome (Leica, Germany) and dried at 37 °C. Deparaffinization and rehydration of the sections were carried out in a series of steps. Firstly, sections were immersed sequentially in three baths of Histo-Clear, followed by two baths of 100% ethanol, followed by 95%, 70%, 50% ethanol baths, for 5 min each. Lastly, the sections were left under running tap water for 10 min. After rehydration, sections underwent antigen retrieval by heating with Tris–EDTA (pH 9.0) at 95 °C for 30 min. Following antigen retrieval, sections were subjected to one of the following procedures: immunofluorescence, immunohistochemistry or H&E staining.

For immunofluorescence staining, sections were blocked with 5% bovine serum albumin (Biowest, France) and 0.1% Triton-X (Sigma Aldrich, USA) for 1 h, followed by overnight incubation with anti-human EGFR antibody (Santa Cruz, Cat #: sc-377073, dilution 1:200) in 5% BSA blocking buffer at 4 °C. The sections were washed with PBS thrice before incubation with goat anti-mouse IgG Alexa-Fluor 488-conjugated antibody (Invitrogen, Cat #: A32723, dilution 1:2000) in 5% BSA blocking buffer for 1 h at room temperature. The sections were also counter-stained with Hoechst 33342 (ThermoFisher Scientific, USA) at a 1:500 dilution and washed three times with PBS. The sections were mounted with anti-fade mounting media (Vector Laboratories, USA) and visualised using an Olympus FV3000 confocal microscope (Olympus, Japan).

For H&E staining, the sections were stained with Mayer's haematoxylin (Abcam, USA) for 1 min. After washing with water, the sections were dipped in 2% ammonia (Sigma Aldrich, USA) twice. The sections were washed with water once and dipped into 70% ethanol 10 times. Subsequently, the sections were stained with alcoholic eosin (Abcam, USA) for 30 s. Following the staining, the sections were dipped in a series of baths, for 10 dips each. Sections were first washed in three baths of 90% ethanol, followed by two baths of 100% ethanol to dehydrate the sections and finally four baths of Histo-Clear to clear the sections. The sections were mounted with DPX Mounting solution (Sigma Aldrich, USA). Images were acquired using an EVOS M7000 Imaging System (ThermoFisher Scientific, USA).

For immunohistochemistry staining, the sections were blocked with 5% bovine serum albumin (Biowest, France) and 0.1% Triton-X-100 (Sigma Aldrich, USA) for 1 h, followed by overnight incubation with anti-human EGFR antibody in 5% BSA blocking buffer at 4 °C. The sections were washed with PBS thrice before incubation with goat anti-mouse HRP-conjugated antibody (Invitrogen, Cat #: 626520, dilution 1:2000) in 5% BSA blocking buffer for 1 h at room temperature. The sections were washed three times with PBS before staining with the SignalStain® DAB Substrate Kit (Cell Signaling Technology), following the manufacturer's instructions. The sections were also counter-stained using the H&E staining protocol as described above.

Apoptosis of cells in lung tissue sections was evaluated using a TUNEL assay Apoptosis Detection Kit (Biotium, USA). Tissue sections were dewaxed in three baths of Histo-Clear (National Diagnostics, USA) for 5 min each, before being dipped in a 1:1 Histo-Clear and 100% ethanol bath. The tissue sections were sequentially rehydrated in 100%, 90%, 75% and 50% ethanol baths before the rehydration in a milliQ water bath. After dewaxing, antigen retrieval was conducted by superheating the sections in a microwave oven at the "High" setting for 15 min, ensuring that the antigen retrieval solution (Tris EDTA buffer, pH 9.0) reached boiling. The sections were left to cool down in the antigen retrieval solution for 30 min. Once cooled, sections were stained with the TUNEL assay kit according to the manufacturer's instructions. Sections were also counter-stained with Hoechst-33342 (Abcam, Cat #: ab228551, dilution 1:200). To reduce auto-fluorescent signals, a Vector® TrueVIEW® Autofluorescence Quenching Kit (Vector Laboratories, USA) was used on the sections according to manufacturer's instructions. Sections were mounted using the VECTASHIELD Vibrance® Anti-fade Mounting Medium (Vector Laboratories) according to manufacturer's instructions. Slides were visualised using an Olympus FV3000 confocal microscope (Olympus). Image acquisition was conducted using the FluoView31S software while further analysis and quantification was conducted using the QuPath-0.4.4 software.

Statistical analysis

Data are presented as the mean ± standard error of the mean (SEM). Each data point corresponds to an independent biological replicate conducted using different passages of cells and/or batches of RBCEVs. All statistical analyses were performed using GraphPad Prism 9 (GraphPad Software, USA). To assess significant differences between the two groups, two-tailed Student's *t*-test was conducted. To assess significant differences between multiple groups, one-way or two-way analysis of variance (ANOVA) was conducted with Tukey's post-hoc test. P-value <0.05 was considered statistically significant, based on at least three independent replicates.

Role of the funding source

The funder played no role in study design, data collection, analysis and interpretation of data, or the writing and submission of this manuscript.

Results

RBCEVs were purified and loaded with ASOs at high efficiency

RBCEVs were purified from human blood using a previously established protocol.[12] The purity of RBCEVs

was confirmed through Western blot analysis (Fig. 1a), which demonstrated enrichment in common EV-specific markers (ALG-2-interacting protein X (ALIX) and Tumour susceptibility gene 101 (TSG101), as well as specific RBCEV surface markers (Glycophorin A (GPA) and Stomatin (STOM)). Notably, the most abundant human RBC membrane proteins (BAND3 anion transport protein and Haemoglobin subunit α (HBA)) were detected, while the expression of cytoskeleton protein β-actin (ACTB) and the endoplasmic reticulum marker Calnexin (CANX) was absent compared to RBCs, indicating the absence of contamination of EVs from other blood cells. Transmission electron microscopy (TEM) analysis further confirmed a homogeneous vesicle-like morphology of isolated RBCEVs (Fig. 1b).

Subsequently, RBCEVs were loaded with ASOs using REG-1 following our previously established protocol.[12] Agarose gel electrophoresis was performed to determine ASO loading efficiency. Fig. 1c & d demonstrated efficient loading, with an approximately loading efficiency of 90%. Further confirmation of successful ASO loading was obtained by quantifying the fluorescence signal of FAM-ASO through nanoflow cytometric analysis (Fig. 1e), showing that 100% of RBCEVs were

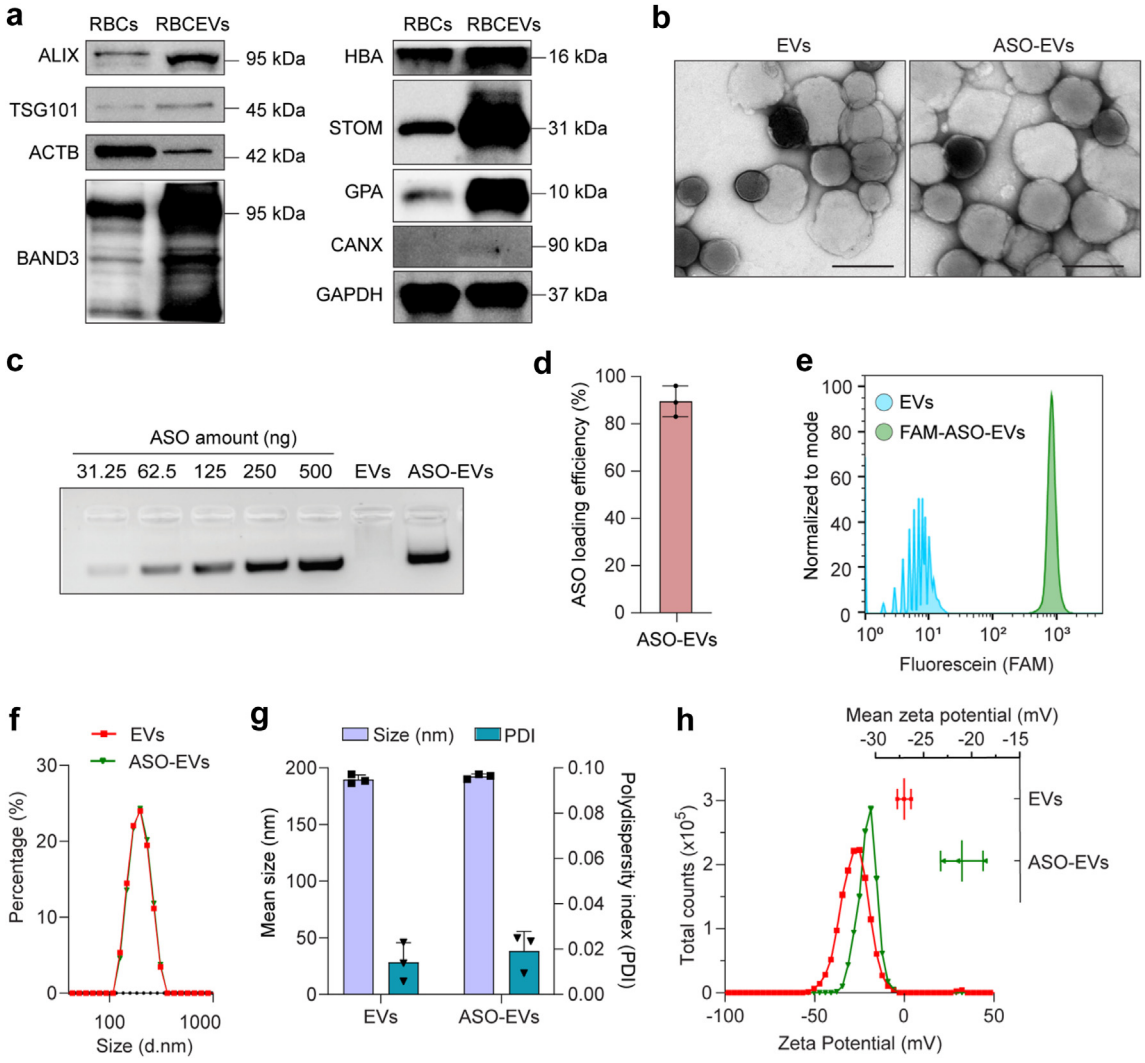

Fig. 1: **Characterization of purified RBCEVs and ASO-loaded RBCEVs.** (**a**) Western blot analysis of ALIX, TSG101, ACTB, STOM, GPA, HBA, BAND3, CANX, and GAPDH protein expression in RBCs and RBCEVs. (**b**) Transmission electron microscopy (TEM) images of RBCEVs (EVs) and ASO-loaded RBCEVs (ASO-EVs) at 40× magnification. Scale bar: 200 nm. (**c-d**) Loading efficiency of negative control ASO (NC ASO) into RBCEVs (ASO-EVs) using REG-1, analysed by agarose gel electrophoresis. (**e**) Nanoflow cytometric analysis of RBCEVs loaded with FAM-ASOs. (**f**) Size distribution of RBCEVs and ASO-loaded RBCEVs (ASO-EVs) determined by dynamic light scattering (DLS). (**g**) Mean size and polydispersity of EVs and ASO-EVs determined by DLS. (**h**) Zeta potential distribution of EVs and ASO-EVs determined by DLS method.

positive for FAM-ASO fluorescence. Dynamic light scattering analysis revealed no significant change in mean size (189.8 nm vs. 192.4 nm respectively) and polydispersity index (0.014 vs. 0.019, respectively) between unloaded RBCEVs and RBCEVs loaded with ASOs (Fig. 1g). Zeta potential measurement indicated an increase in RBCEVs membrane charge from –27 mV to –21 mV when RBCEVs were loaded with ASOs (Fig. 1h). These data suggest the successful production of highly purified, homogeneous RBCEVs, and demonstrate successful ASO loading without compromising the original physicochemical characteristics.

Specific knockdown of mutant genes in NSCLC using ASO-loaded RBCEVs

We received three tumour samples from patients with NSCLC (Fig. S1). Based on the genetic profiling data from patient-derived cancer samples, we found either *EGFR* L858R or T790M mutations present. We therefore designed and screened for ASOs that specifically inhibit these mutants. ASOs were designed using a Gapmer approach and chemically modified with locked nucleic acid (LNA), phosphorothioate (PS), and 2′-O-methoxyethyl (2′MOE) to increase the stability and specificity of the ASOs (Fig. 2a).

To examine the ability of RBCEVs to deliver ASOs to lung cancer cells, we loaded RBCEVs with a fluorophore-labelled ASO and investigated the uptake of ASO-loaded RBCEVs by H1975 human lung cancer cells using flow cytometry and confocal microscopy. We observed that the RBCEVs could efficiently deliver the ASOs into cancer cells within a few hours of incubation (Fig. S2), suggesting that RBCEVs are suitable for ASO delivery to lung cancer cells.

We subsequently examined the specific knockdown of *EGFR* with L858R and T790M mutations in H1975 cells, given that these cells carry both mutations (Fig. S3a). A549 cells that express WT *EGFR* were used as a control cell line. Through qPCR and Western blot analysis, we demonstrated that RBCEV-delivered *EGFR* L858R ASO3 and T790M ASO4 specifically inhibited *EGFR* expression at both the mRNA and protein levels in target cells, with limited effect on the WT *EGFR* in A549 control cells (Fig. 2b–e). Based on these data, we selected L858R ASO3 and T790M ASO4 for downstream studies. Importantly, the mutant-specific ASOs delivered by RBCEVs noticeably reduced the growth of mutant-bearing cells as determined by the CCK-8 assay, while minimising cross-reaction in WT gene-harbouring A549 cells (Fig. S3b and c). We further examined if the selected ASOs cause any off-target effects by analysing the expression of genes with at least 70% sequence matching to the sequences of L858R ASO3 (*FMR1*, *TRMT11*, and *POU2F3*) and T790M ASO4 (*FRY* and *TFEB*). Fig. S3d and e showed no significant changes in the expression of these genes, confirming the specificity of the selected ASOs. Notably, the treatment with RBCEVs loaded with these EGFR mutant-specific ASOs remarkably decreased the expression of proteins associated with two primary EGFR downstream effectors, including AKT and ERK1/2 (Fig. S3f). These results indicate that RBCEVs are a suitable platform for delivering ASOs to cancer cells, and utilising the oncogene-specific ASOs is a promising approach for cancer treatment as they can specifically inhibit driver mutations in cancer cells while sparing the normal WT genes.

Mutant-specific ASOs delivered by RBCEVs exhibit potent anti-cancer effects in TKI-resistant NSCLC cells

We next aimed to compare the anti-tumour activity of our ASO-loaded RBCEVs with three FDA-approved generations of TKIs, including Icotinib, Afatinib, and Osimertinib. Initially, we assessed the effects of Icotinib, a first-generation TKI, and Osimertinib, a third-generation TKI, on EGFR in H1975 cells, which possess the L858R/T790M co-mutation, through Western blot analysis. As shown in Fig. S4, only Osimertinib reduced the level of phosphorylated EGFR in H1975 cells. We next examined the apoptosis induction in H1975 cells treated with Icotinib, Afatinib, and Osimertinib, L858R ASO-EVs, and T790M ASO-EVs, each at a drug concentration of 200 nM, by staining the treated cells with Annexin V and SYTOX Blue reagent. As shown in Fig. 3a–b, L858R ASO-EVs and T790M ASO-EVs outperformed all TKIs in inducing various stages of apoptosis, namely early apoptosis (Annexin V^+, SYTOX $Blue^-$), necrosis (Annexin V^-, SYTOX $Blue^+$), and late apoptosis (Annexin V^+, SYTOX $Blue^+$).

Subsequently, we treated H1975 cells with various doses of TKIs and ASOs loaded in RBCEVs and analysed cell numbers after 48 h using the CCK8 assay (Fig. 3c). Consistent with the flow cytometric analysis of apoptosis, the delivery of L858R ASO and T790M ASO by RBCEVs at 200 nM significantly suppressed the growth of H1975 cells, surpassing the efficacy of all three generations of TKIs. This indicates that our ASOs, targeting mutations at the mRNA level, confer advantages over small molecules targeting the EGFR protein in terms of anti-tumour efficacy.

Conjugation of RBCEVs with anti-EGFR nanobody promotes targeted delivery of ASOs to lung cancer cells

We developed a simple and efficient method for conjugating α-EGFR-VHHs (specific to human EGFR) to RBCEVs using copper-free DBCO-azide cycloaddition-based click chemistry (Fig. 4a). Initially, we modified the RBCEV surface with reactive Dibenzocyclooctyne (DBCO-EVs) group and the α-EGFR-VHH with azide (Azido VHH) using DBCO-conjugated 4-Sulfo-2,3,5,6-tetrafluorophenyl (STP) ester and 6-Azidohexanoic acid-conjugated STP ester, respectively. The subsequent

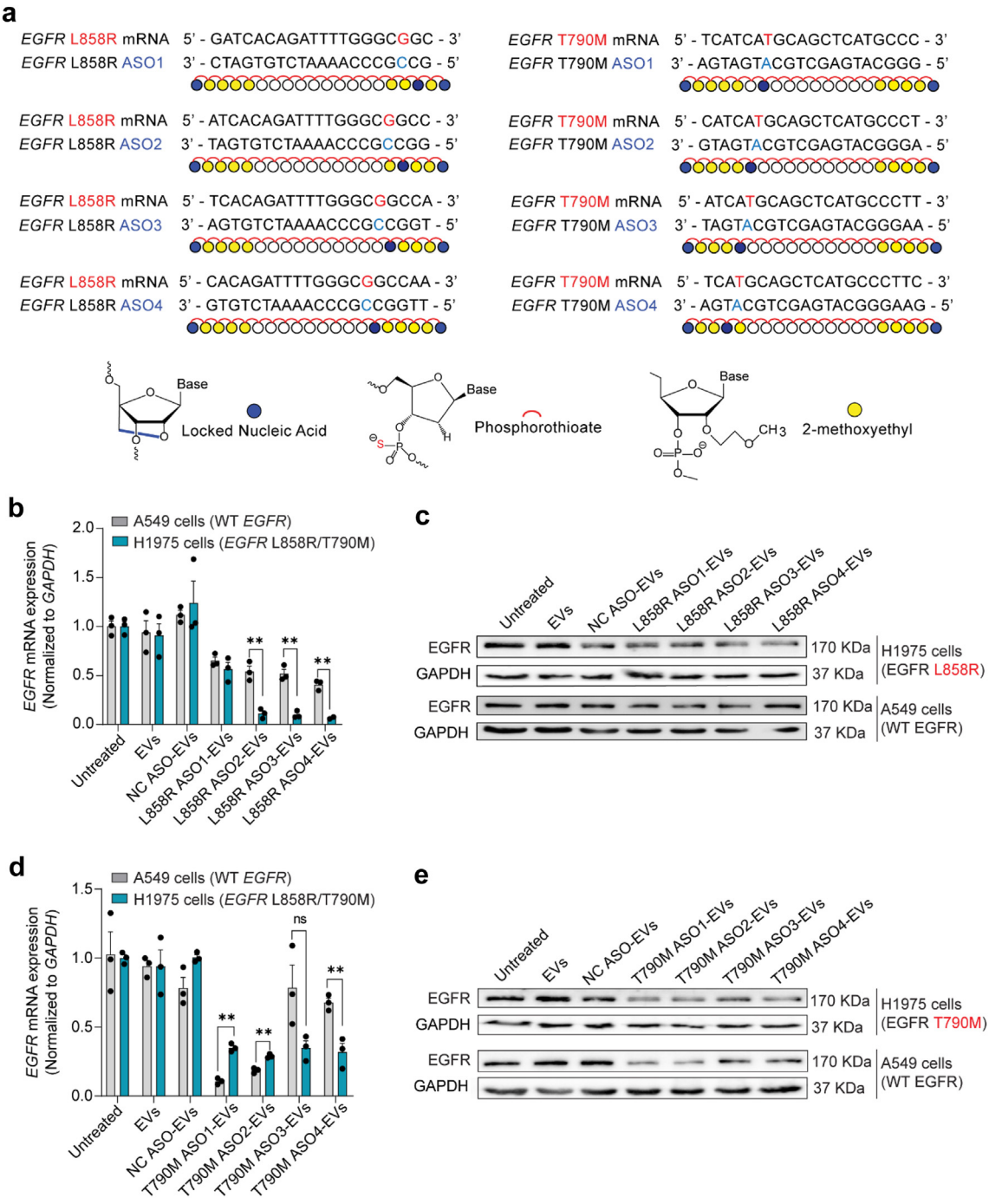

***Fig. 2:* Antisense oligonucleotides (ASOs) are designed to specifically inhibit *EGFR* L858R/T790M mutants.** **(a)** Sequences and chemical modifications of anti-*EGFR* L858R and anti-*EGFR* T790M ASOs. (**b**–**e**) Knockdown of *EGFR* in H1975 cells bearing *EGFR* L858R/T790M mutations and A549 cells with wild-type *EGFR* two days following treatment with unloaded or ASO-loaded RBCEVs, as determined by qPCR (**b**, **d**) and Western blot analysis (**c**, **e**) (n = 3). The graphs present the mean ± SEM (n = 3 biological replicates). ns – not significant, *P < 0.05, **P < 0.01, and ***P < 0.001, determined by Student's two-tailed t-test.

click reaction between DBCO-modified RBCEVs and azido-modified VHHs resulted in nanobody-conjugated EVs (VHH-EVs). Western blot analysis confirmed the successful conjugation of the nanobody onto RBCEVs, resulting in an average of ~200 copies of α-EGFR-VHH per RBCEV (Fig. S5a and b). Importantly, the conjugation

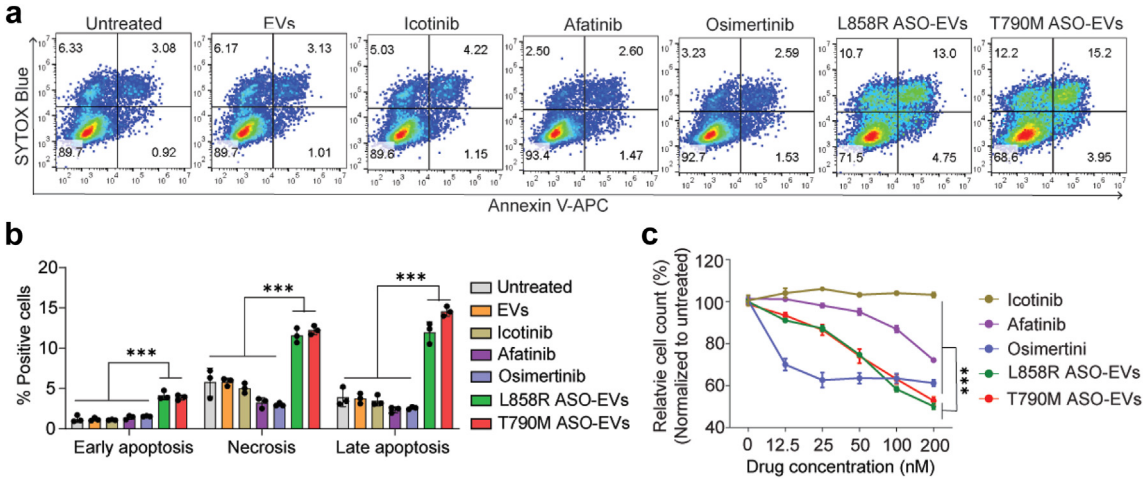

Fig. 3: **RBCEVs loaded with *EGFR* mutant-specific ASOs exhibit superior anti-cancer effect compared to TKIs.** (**a**) Flow cytometric analysis of Annexin V/SYTOX Blue staining in H1975 cells 24 h post-treatment with 200 nM of Icotinib, Afatinib, Osimertinib, unloaded RBCEVs (EVs) or ASO-loaded RBCEVs (L858R ASO-EVs, T790M ASO-EVs). (**b**) Proportion of early apoptotic (Annexin$^+$, SYTOX Blue$^-$), necrotic (Annexin$^-$, SYTOX Blue$^+$), and late apoptotic (Annexin$^+$, SYTOX Blue$^+$) H1975 cells treated as described in (A) (n = 3). (**c**) Relative cell counts of H1975 cells two days after treatment with Icotinib, Afatinib, Osimertinib, unloaded RBCEVs or ASO-loaded RBCEVs at equal concentrations as shown in (a), determined by the CCK8 assay (n = 3 biological repeats). The graphs present mean ± SEM. ***P < 0.001, determined using One-Way ANOVA test.

with α-EGFR-VHH did not significantly alter the size and charge of the RBCEVs (Fig. S5c–e).

To assess the specificity of EGFR-targeting RBCEVs towards EGFR-expressing lung cancer cells, α-EGFR-VHH-conjugated RBCEVs were labelled with Aco-490 dye and incubated with H1975 cells, which highly express EGFR. Mouse 4T1 breast cancer cells transduced with a lentivirus carrying a human EGFR expression vector (4T1-EGFR) were used as a positive control, while parental 4T1 cells were used as a negative control. To ensure that any observed effects on cellular uptake were not attributed to the conjugation process itself, RBCEVs were also conjugated with an anti-mCherry nanobody and used as negative control EVs (Ctrl-VHH-EVs). Flow cytometric analysis revealed that α-EGFR-VHH ligation on the RBCEV surface significantly promoted the EV uptake by H1975 and 4T1-EGFR cells, but not by parental 4T1 cells (Fig. 4b–e).

Subsequently, we sought to confirm whether the conjugation with α-EGFR-VHH could enhance the specific delivery of ASO-loaded RBCEVs to lung tumour cells *in vivo*. To quantify tumour progression in live mice, we transduced H1975 lung cancer cells with a lentivirus carrying reporter genes encoding luciferase and mCherry (H1975-Luc-mCherry cells) (Fig. S6). The resulting cells were injected intravenously into NSGS mice, and tumour growth in the lungs was monitored using an *in vivo* imaging system (IVIS) (Fig. 4f). We next delivered non-targeted and EGFR-targeted RBCEVs loaded with FAM-ASO via intratracheal administration to the mice bearing H1975-Luc-mCherry-tumours. Three hours post-intratracheal delivery, the ability of non-targeted and EGFR-targeted RBCEVs in delivering ASO to tumour cells was analysed. Flow cytometric analysis showed that the conjugation of RBCEVs with α-EGFR-VHH increased the delivery of ASO to lung cancer cells, as indicated by the elevated fluorescent intensity of FAM-ASO in H1975-Luc-mCherry tumour cells (Fig. 4g). This data suggests that α-EGFR-VHH conjugation can enhance specific delivery of ASO-loaded RBCEVs to lung cancer cells *in vivo*.

Targeted delivery of mutant-specific ASOs via RBCEVs conjugated with EGFR-binding nanobodies enhances anti-cancer efficacy

We first examined if intratracheal delivery of ASO-loaded EVs could significantly inhibit tumour growth in the lungs. We generated an orthotopic lung cancer model using H1975-Luc-mCherry tumour cells as described above and treated the tumour-bearing mice every three days with EVs loaded with either NC ASO or T790M ASO (Fig. S7a). We observed that T790M ASO-loaded EVs exhibited a markedly higher anti-cancer effect compared to NC ASO-loaded EVs (Fig. S7b and c). Furthermore, the expression of EGFR at the tumour area was significantly decreased in the mice that received T790M ASO treatment (Fig. S7d). We further investigated whether our EGFR-targeted delivery strategy improves the overall efficacy of ASOs in inhibiting cancer growth compared to untargeted delivery. L858R ASO was loaded into unconjugated RBCEVs or EGFR-VHH-EVs and delivered to H1975-Luc-mCherry tumour-bearing mice intratracheally every 3 days (Fig. 5a). L858R-ASO-loaded RBCEVs exhibited a significant tumour inhibitory effect, with a lower luciferase

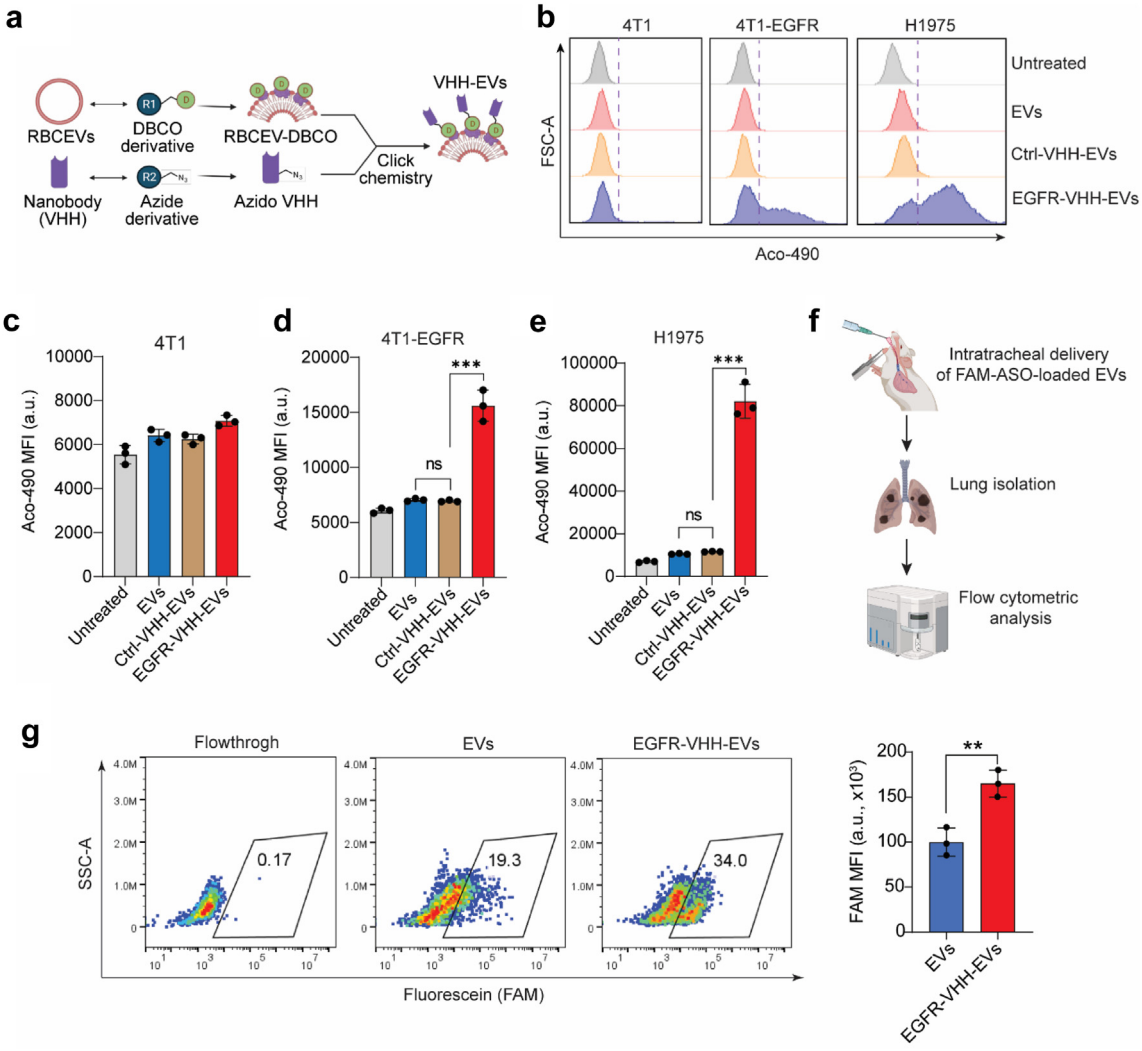

Fig. 4: **Conjugation of RBCEVs with anti-EGFR nanobody promotes targeted delivery of ASOs to lung cancer cells.** (**a**) Schematic for anti-EGFR nanobody (α-EGFR-VHH) conjugation onto RBCEV surface by copper-free DBCO-azide cycloaddition-based click chemistry. (**b**) Flow cytometric analysis reflecting the uptake of Aco-490-labelled RBCEVs ligated with α-EGFR-VHH by 3 tumour cell lines, including human lung cancer H1975 cells, mouse breast cancer 4T1 cells, human EGFR-expressing 4T1 cells (4T1-EGFR). (**c-e**) Mean fluorescence intensity (MFI) of Aco-490 in each cell line after incubation with Aco-490-labelled RBCEVs, including RBCEVs conjugated with α-mCherry nanobody (Ctrl-VHH-EVs) or α-EGFR nanobody (EGFR-VHH-EVs) (n = 3). (**f**) Schematic for intratracheal delivery of RBCEV formulations in NSGS mice bearing lung tumours, generated by injection of H1975-Luc-mCherry cells into the tail vein. (**g**) Flow cytometric analysis of FAM-ASO signal in tumour cells isolated from the lungs of H1975 tumour-bearing mice treated with unconjugated and EGFR nanobody-conjugated RBCEVs (VHH-EVs) loaded with FAM-ASO (n = 3). The graphs present the mean ± SEM. ns – not significant, **P < 0.01, ***P < 0.001 determined by Student's two-tailed t-test.

signal compared to mice receiving NC ASO-loaded EVs. Remarkably, modifying the RBCEV surface with α-EGFR-VHH further enhanced the anti-cancer effect of the ASO (Fig. 5b–c). Importantly, there was no noticeable toxicity observed in the treated mice, evidenced by the steady maintenance of body weight throughout the treatment course (Fig. 5d). We then examined whether L858R ASO delivered by EGFR-targeted-EVs could suppress EGFR expression in lung tumours. Through immunohistochemistry (IHC) staining, we observed the most noticeable decrease in EGFR protein levels in the L858R ASO-VHH-EV-treated group, compared to mice treated with NC ASO-EVs and L858R ASO-EVs (Fig. 5e). Collectively, these data indicate that targeted delivery via α-EGFR-VHH-EVs to cancer cells results a higher anti-cancer efficacy of mutant-targeting ASOs.

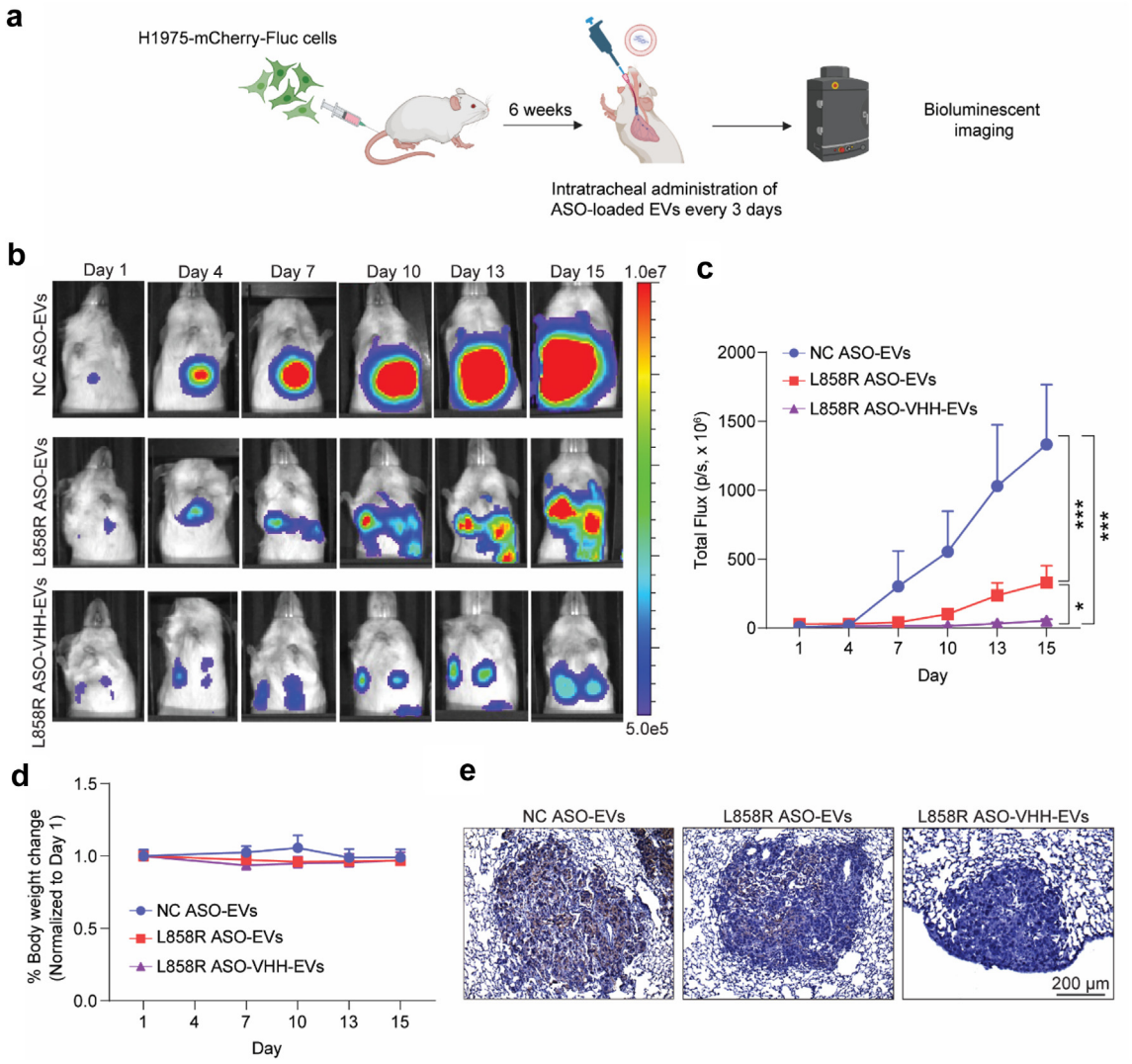

Fig. 5: **Conjugation of RBCEVs with anti-EGFR nanobody enhances anti-cancer efficacy of RBCEV-delivered ASOs.** (**a**) Schematic for intratracheal treatment of H1975-Luc-mCherry tumours in NSGS mice with different RBCEV formulations. (**b**) Representative bioluminescent images of xenograft mice treated with NC ASO-EVs, L858R ASO-EVs or L858R ASO-VHH-EVs over time. (**c**) Tumour progression in mice was quantified using the average bioluminescent signals following treatment with NC ASO-EVs, L858R ASO-EVs, or L858R ASO-VHH-EVs over time (n = 4 mice). **(d)** Percentage of change in mouse body weight documented through the course of treatment. (**e**) Representative IHC images of EGFR protein expression (brown) in lung tissues of treated tumour-bearing mice at the end of study. The graphs present the mean ± SEM. *P < 0.05, ***P < 0.001 determined by two-way ANOVA.

EGFR mutant-specific ASO-loaded RBCEVs effectively inhibit the growth of TKI-resistant patient-derived tumour cells

Given that cell line-based xenografts have limited ability to predict therapeutic responses in clinical settings and are generated from a limited number of cell lines, they are thus unable to fully represent the phenotypic diversity apparent in human disease. These shortcomings can be addressed by using the patient-derived xenograft (PDX) model as it retains morphological properties of the original tumour specimen, and any metastatic potential from the implantation site. Importantly, PDXs closely reflect sensitivity to anti-cancer drugs and the clinical outcome of patients with cancer owing to the carried-over tumour stroma and replicated murine stroma.[16] It is also noteworthy that PDXs have consistent biological properties and stable phenotypes across multiple passages, allowing for the characterization of genetic mutations present in a specific tumour via genome sequencing and gene expression profiling, which may open up the possibility of personalised therapy.[17] Therefore, we examined anti-cancer potency

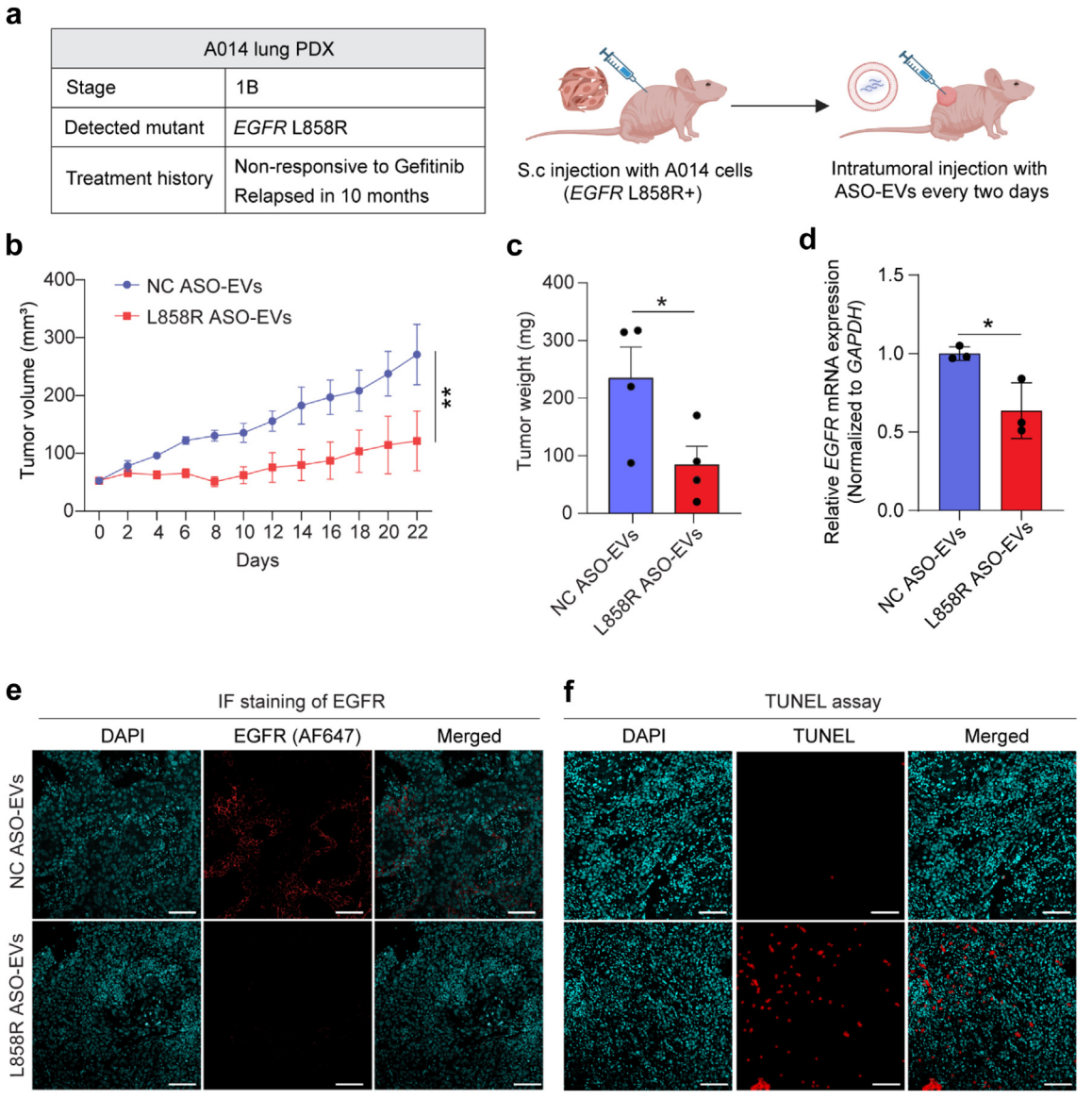

***Fig. 6: EGFR* L858R ASO-loaded RBCEVs effectively inhibit the growth of lung tumours in a patient-derived xenograft mouse model with *EGFR* mutation**. (**a**) Characteristics of A014 patient-derived lung cancer cells and schematic treatment of A014 tumour in BALB/c nude mice with intra-tumoural injection of NC ASO-EVs or L858R ASO-EVs. (**b**) Tumour volume of the A014 tumour-bearing mice over time after the treatment (n = 4 mice). (**c**) Weight of tumour masses collected from treated mice at sacrifice. (**d**) *EGFR* mRNA expression in tumours from mice treated with NC ASO- EVs or L858R ASO-EVs examined by qPCR at the end of study. (**e**) Representative immunofluorescent images of EGFR staining in tumour sections from treated mice at the end of the study, scale bar 100 μm. (**f**) Representative TUNEL staining images of tumour sections from treated mice at the end of the study, scale bar 100 μm. The graphs present the mean ± SEM. *P < 0.05, **P < 0.01 determined by two-way ANOVA (b) or Student's two-tailed t-test (d).

of ASO-loaded EVs in a PDX model generated by inoculating A014 tumour cells, collected from a patient with NSCLC who was unresponsive to Gefitinib treatment, into BALB/c nude mice (Fig. 6a). Eight mice with similar tumour sizes were divided into two groups, after which they received intra-tumoural injections of either L858R ASO-EVs (n = 4), or NC ASO-EVs (n = 4) as a negative control. We observed extensively delayed tumour growth when mice were injected with L858R ASO-EVs compared to those treated with NC ASO-loaded EVs, indicated by a significantly lower tumour volume (Fig. 6b) and tumour weight (Fig. 6c). To shed light on the anti-cancer activity of L858R ASO-EVs, we conducted qPCR analysis and immunofluorescent staining to determine EGFR levels in the tumours of treated mice. We observed marked reduction in EGFR at

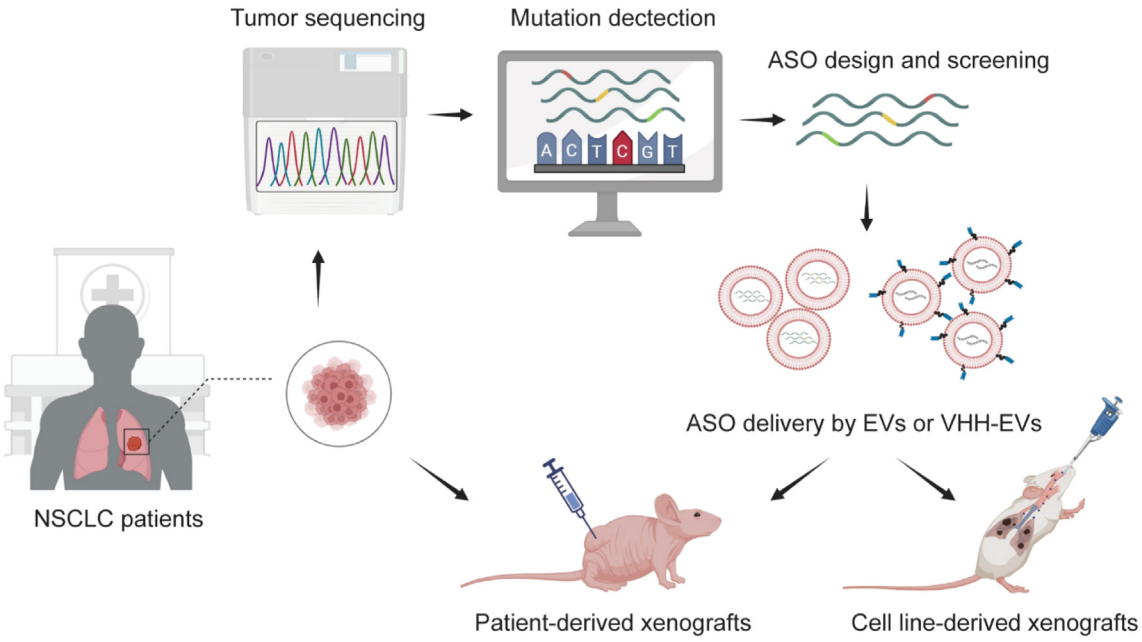

Fig. 7: **Personalised treatment of NSCLC utilising ASOs delivered by RBCEVs**. Patient tumours are collected, and tumour cells are sequenced to uncover the mutation profile. ASOs are designed for targeting oncogenic driver mutations and delivered to tumour cells by RBCEVs. The surface of RBCEVs is engineered with tumour-targeting nanobodies to improve their homing to target site and internalization into target cells. The ASO-VHH-EVs platform is subsequently tested on cell line- and patient-derived xenografts for their safety, biodistribution and therapeutic efficiency.

both mRNA (Fig. 6d) and protein levels (Fig. 6e) in EV-L858R ASO-treated mice compared to those treated with NC ASO-EVs. Additionally, we performed a TUNEL assay to detect apoptosis in PDX tumours. Fig. 6f showed a remarkably increased number of TUNEL-positive cells within tumours of mice that received L858R ASO-EVs, demonstrating the anti-tumour potency of this platform (Fig. 7).

The anti-cancer efficacy of T790M ASO-loaded EVs *in vitro* was further confirmed in A003 tumour cells derived from a patient with NSCLC. This patient had previously received three lines of treatment, including afatinib, a combination of carboplatin and pemetrexed, and a dual PI3K/MEK inhibition therapy. Our results demonstrated that EVs delivered with T790M ASO effectively inhibited EGFR expression (Fig. S8a and b), reduced cell counts (Fig. S8c), and induced tumour cell death (Fig. S8d and e).

These results demonstrate that our approach of utilising ASOs tailored to specific mutations of individual patients with NSCLC holds promise of improving treatment outcomes and addressing challenges associated with resistance to small molecule drugs in cancer therapy.

Discussion

NSCLC driven by oncogenic *EGFR* mutations exhibits a particularly high prevalence.[18] Various combination therapies are being investigated in clinical trials as alternative interventions for patients with EGFR TKI-resistant NSCLC, pending the development of an effective next-generation TKI or other management strategies.[19] Hence, NSCLC treatments may benefit from the development of new modalities such as nucleic therapeutics. Recently, tremendous attention has been directed to nucleic acid therapeutics, including aptamers, small interference RNAs (siRNAs), and antisense oligonucleotides (ASOs), due to their great potential in specifically inhibiting currently undruggable targets. Compared to other therapeutic agents, such as small molecules, antibodies, and peptides, ASO drugs offer numerous advantages. Firstly, the screening, designing, and synthesising ASOs are much less time-consuming and more cost-effective than that required for chemical and protein drugs.[20] Secondly, chemical modifications of ASOs are quick and simple.[21] Thirdly, the effect of ASOs is typically limited to mutant-harbouring cells, thus lowering risks of side effects.[22,23] However, their highly anionic nature and susceptibility to serum nucleases make it difficult for ASOs to enter cells efficiently and function on their own.

Viral vector and non-viral delivery systems using synthetic materials have been employed to overcome barriers to safe and efficient nucleic acid delivery. However, effectiveness of virus-based delivery is limited due to viral-induced immunogenicity, unwanted genomic integration, and inability to re-dose.[24] With

rapid advances in material sciences and nanotechnology, synthetic nanoparticle delivery systems have shown potential in clinical gene therapy. However, the use of synthetic nanoparticles typically involves complex technologies, high cost of scaling-up production, and potential systemic toxicity.[25] Recently, our group has successfully developed an efficient platform for nucleic acid delivery using RBCEVs. We have demonstrated that RBCEVs can be isolated with high yield (up to 10^{14} EVs per unit of blood) and high purity.[12] Notably, RBCEVs are quickly internalised by various cancer cell types, including lung cancer, acute myeloid leukeemia, and breast cancer cells.[13,26,27] We are able to load a wide range of nucleic acids, including ASOs, siRNAs, immunomodulatory RNAs, gRNAs, and Cas9 mRNAs, into RBCEVs and effectively deliver them into cancer cells both *in vitro* and *in vivo*.[12,26,28]

In this study, we aimed to capitalise on the advantages of ASOs to target activating *EGFR* mutations inherent to NSCLC in an individualised manner (Fig. 7). This includes the notorious activating *EGFR* mutations, L858R and T790M, which confers resistance to tumours treated with 1st and 2nd generation TKIs. Given that all activating *EGFR* mutations are associated with the ATP-binding pocket, which is the binding site for TKIs,[29] targeting *EGFR* mutants at the mRNA level by ASOs can overcome any acquired resistance associated with EGFR mutants and TKIs. The versatility of ASO design and the rapid ASO synthesis process are remarkable advantages of the ASO approach for combating drug-resistant mutations in cancer. By complexing with RBCEVs, personalised ASOs were efficiently internalised into cancer cells and robustly suppressed *EGFR* expression in mutant tumour cells, while sparing the normal WT gene. Notably, in a parallel comparison, we found that both L858R and T790M ASOs could suppress the growth of lung cancer cells bearing L858R/T790M co-mutations more effectively than FDA-approved EGFR TKIs at equivalent doses.

More importantly, the ASO-loaded RBCEVs strongly inhibited the growth of PDX tumours generated from a patient who experienced a relapse in cancer development and resistant to EGFR TKI-treatments, suggesting the advantages of our approach over the small molecule approach in targeting point mutations for cancer treatment.

Although RBCEVs are generally biocompatible, it is important to test potential side effects of the formulated RBCEVs. A limitation of our study is the lack of a long-term toxicity test. While we did not observe any noticeable toxicity in mice treated with ASO-loaded RBCEVs, multiple doses of human RBCEVs over a longer period could potentially trigger an immune response in the mouse model due to the reactions of the mice to human proteins on RBCEVs. Purification of mouse RBCEVs is challenging because of the small blood volume and the fragile characteristics of mouse RBCs. For a long-term toxicity study, we will need to identify another animal model that is more suitable than mice.

Another limitation of EV-based delivery is the routes of administration. In our project, we utilized intratracheal or intratumoural administration of ASO-loaded EVs instead of intravenous administration due to the short half-life of RBCEVs in the bloodstream, where they are cleared by the reticuloendothelial system (RES). In a clinical setting, we could deliver the ASO-loaded RBCEVs to the lungs of a patient with lung cancer via inhalation. Systemic treatment of cancer metastasis would require more development of the platform to improve the half-life and biodistribution of RBCEVs.

Contributors

All authors read, revised, and approved the final manuscript. T.T.T.T, C.D.P, and B.Z.J.Y have accessed and verified all the underlying data. T.T.T.T, C.D.P, and B.Z.J.Y designed and performed the majority of experiments, made significant contributions to manuscript preparation and verified all data. R.C.P performed the *in vitro* assays comparing the anti-cancer effect of TKIs with the designed ASOs and contributed to manuscript writing. M.K.J developed the method for the conjugation of the nanobody onto EV's surface, provided guidance on this procedure, and contributed to data analysis. E.Y.M.Y conducted IF staining of EGFR and performed TUNEL assays to detect apoptotic cells in lung tissues. J.Y and D.S.W.T maintained and provided PDX cell lines and contributed to manuscript proofreading. B.C.G advised on target selection for the study and provided guidance on the project's direction. M.T.N.L and W.L.T initiated the research, obtained funding, coordinated the group, managed the project, and revised the manuscript.

Data sharing statement

All data from this study are available upon reasonable request to the corresponding authors.

Declaration of interests

M.T.N.L is a cofounder and advisor of Carmine Therapeutics, which develops gene therapy, and has a patent relating to Vesicle-Based Compositions and Uses Thereof. Carmine Therapeutics provides a proprietary transfection reagent required for loading of ASOs into EVs used in this study.

C.D.P has a patent relating to Vesicle-Based Compositions and Uses Thereof.

M.K.J has received consulting fees from Jotbody HK Ltd and patent royalties from Carmine Therapeutics. He also has two pending patents filed with NUS ILO and NTUITIVE pertaining to EVs.

B.C.G has a patent relating to Modulation of Signal Transducer and Activator of Transcription 3 (STAT3) Expression.

D.S.W.T has received grants from ACM Biolabs, Amgen, Astra Zeneca, Bayer and Pfizer, consulting fees from Amgen, Astra Zeneca, Bayer, Boehringer Ingelheim, DKSH, GlaxoSmithKline, Merck, Novartis, Pfizer, Roche and Takeda, honoraria from Amgen, Bayer, Merck, Pfizer, Novartis, Boehringer Ingelheim, Roche, Takeda, BeiGene, Regeneron and Zymeworks. He has also obtained support for travel from Bayer, Merck, Pfizer, Regeneron and Zymeworks.

Other authors declare no competing financial interest.

Acknowledgements

This study was funded by Singapore Ministry of Health, National Medical Research Council (NMRC/OFIRG/MOH-000643-00, NMRC/OFLCG/002-2018, OFIRG21nov-0068, OFYIRG22jul-0034), National Research Foundation, Singapore (NRF-NRFI08-2022, NRF-CRP22-2019-0003, NRF-CRP23-2019-0004), Agency for Science, Technology and Research, Singapore (A*STAR), and the Singapore Ministry of Education under its Research Centres of Excellence initiative. We would like to acknowledge Carmine Therapeutics for providing essential reagents and support. We also thank our colleagues, A/Prof. Luo Dahai and Nguyen

Mai Trinh (Lee Kong Chian School of Medicine, Nanyang Technological University, Singapore) for providing nanobodies and advice. Additionally, we extend our appreciation to A/Prof. Gautam Sethi, and A/Prof. Polly Chen, for valuable advice, to Jonetta Pek, Wen Xiu Loh, Gao Chang, Xuan Dang, Hong Anh Le, and Yock Sin Lay for their assistance. Schematics were created using BioRender.com. During the preparation of this work, the authors used Chat GPT (OpenAI) to proofread the manuscript. After using this tool, the authors reviewed and edited the content as needed and take full responsibility for the content of the publication.

Appendix A. Supplementary data

Supplementary data related to this article can be found at https://doi.org/10.1016/j.ebiom.2024.105356.

References

1 Ganti AK, Klein AB, Cotarla I, Seal B, Chou E. Update of incidence, prevalence, survival, and initial treatment in patients with non–small cell lung cancer in the US. *JAMA Oncol*. 2021;7(12):1824–1832.
2 Weinstein IB. Cancer. Addiction to oncogenes–the Achilles heal of cancer. *Science*. 2002;297(5578):63–64.
3 Cross DA, Ashton SE, Ghiorghiu S, et al. AZD9291, an irreversible EGFR TKI, overcomes T790M-mediated resistance to EGFR inhibitors in lung cancer. *Cancer Discov*. 2014;4(9):1046–1061.
4 Westover D, Zugazagoitia J, Cho BC, Lovly CM, Paz-Ares L. Mechanisms of acquired resistance to first- and second-generation EGFR tyrosine kinase inhibitors. *Ann Oncol*. 2018;29:i10–i19.
5 Yu HA, Arcila ME, Rekhtman N, et al. Analysis of tumor specimens at the time of acquired resistance to EGFR-TKI therapy in 155 patients with EGFR-mutant lung cancers. *Clin Cancer Res*. 2013;19(8):2240–2247.
6 Soria JC, Ohe Y, Vansteenkiste J, et al. Osimertinib in untreated EGFR-mutated advanced non-small-cell lung cancer. *N Engl J Med*. 2018;378(2):113–125.
7 Leonetti A, Sharma S, Minari R, Perego P, Giovannetti E, Tiseo M. Resistance mechanisms to osimertinib in EGFR-mutated non-small cell lung cancer. *Br J Cancer*. 2019;121(9):725–737.
8 Hirsch FR, Redman MW, Moon J, et al. EGFR high copy number together with high EGFR protein expression predicts improved outcome for cetuximab-based therapy in squamous cell lung cancer: analysis from SWOG S0819, a phase III trial of chemotherapy with or without Cetuximab in advanced NSCLC. *Clin Lung Cancer*. 2022;23(1):60–71.
9 Kulkarni JA, Witzigmann D, Thomson SB, et al. The current landscape of nucleic acid therapeutics. *Nat Nanotechnol*. 2021;16(6):630–643.
10 Wurster CD, Ludolph AC. Nusinersen for spinal muscular atrophy. *Ther Adv Neurol Disord*. 2018;11:1756285618754459.
11 Herrmann IK, Wood MJA, Fuhrmann G. Extracellular vesicles as a next-generation drug delivery platform. *Nat Nanotechnol*. 2021;16(7):748–759.
12 Usman WM, Pham TC, Kwok YY, et al. Efficient RNA drug delivery using red blood cell extracellular vesicles. *Nat Commun*. 2018;9(1):2359.
13 Pham TC, Jayasinghe MK, Pham TT, et al. Covalent conjugation of extracellular vesicles with peptides and nanobodies for targeted therapeutic delivery. *J Extracell Vesicles*. 2021;10(4):e12057.
14 Jayasinghe MK, Pirisinu M, Yang Y, et al. Surface-engineered extracellular vesicles for targeted delivery of therapeutic RNAs and peptides for cancer therapy. *Theranostics*. 2022;12(7):3288–3315.
15 Liu X, Ory V, Chapman S, et al. ROCK inhibitor and feeder cells induce the conditional reprogramming of epithelial cells. *Am J Pathol*. 2012;180(2):599–607.
16 Yoshida GJ. Applications of patient-derived tumor xenograft models and tumor organoids. *J Hematol Oncol*. 2020;13(1):4.
17 Hidalgo M, Bruckheimer E, Rajeshkumar NV, et al. A pilot clinical study of treatment guided by personalized tumorgrafts in patients with advanced cancer. *Mol Cancer Ther*. 2011;10(8):1311–1316.
18 Chevallier M, Borgeaud M, Addeo A, Friedlaender A. Oncogenic driver mutations in non-small cell lung cancer: past, present and future. *World J Clin Oncol*. 2021;12(4):217–237.
19 Johnson M, Garassino MC, Mok T, Mitsudomi T. Treatment strategies and outcomes for patients with EGFR-mutant non-small cell lung cancer resistant to EGFR tyrosine kinase inhibitors: focus on novel therapies. *Lung Cancer*. 2022;170:41–51.
20 Roberts TC, Langer R, Wood MJA. Advances in oligonucleotide drug delivery. *Nat Rev Drug Discov*. 2020;19(10):673–694.
21 Deleavey GF, Damha MJ. Designing chemically modified oligonucleotides for targeted gene silencing. *Chem Biol*. 2012;19(8):937–954.
22 Boros BD, Schoch KM, Kreple CJ, Miller TM. Antisense oligonucleotides for the study and treatment of ALS. *Neurotherapeutics*. 2022;19(4):1145–1158.
23 Carroll JB, Warby SC, Southwell AL, et al. Potent and selective antisense oligonucleotides targeting single-nucleotide polymorphisms in the Huntington disease gene/allele-specific silencing of mutant huntingtin. *Mol Ther*. 2011;19(12):2178–2185.
24 Paunovska K, Loughrey D, Dahlman JE. Drug delivery systems for RNA therapeutics. *Nat Rev Genet*. 2022;23(5):265–280.
25 Wong JKL, Mohseni R, Hamidieh AA, MacLaren RE, Habib N, Seifalian AM. Limitations in clinical translation of nanoparticle-based gene therapy. *Trends Biotechnol*. 2017;35(12):1124–1125.
26 Peng B, Nguyen TM, Jayasinghe MK, et al. Robust delivery of RIG-I agonists using extracellular vesicles for anti-cancer immunotherapy. *J Extracell Vesicles*. 2022;11(4):e12187.
27 Chen H, Jayasinghe MK, Yeo EYM, et al. CD33-targeting extracellular vesicles deliver antisense oligonucleotides against FLT3-ITD and miR-125b for specific treatment of acute myeloid leukaemia. *Cell Prolif*. 2022;55(9):e13255.
28 Pham TT, Chen H, Nguyen PHD, Jayasinghe MK, Le AH, Le MTN. Endosomal escape of nucleic acids from extracellular vesicles mediates functional therapeutic delivery. *Pharmacol Res*. 2023;188:106665.
29 Gazdar AF. Activating and resistance mutations of EGFR in non-small-cell lung cancer: role in clinical response to EGFR tyrosine kinase inhibitors. *Oncogene*. 2009;28 Suppl 1(Suppl 1):S24–S31.